Differential modes of crosslinking establish spatially distinct regions of peptidoglycan in *Caulobacter crescentus*

Running title: Distinct domains of peptidoglycan in *C. crescentus*

Gabriele Stankeviciute[1], Amanda V. Miguel[2], Atanas Radkov[3], Seemay Chou[3,5], Kerwyn Casey Huang[2,4,5], and Eric A. Klein[1,6,#]

[1]Center for Computational and Integrative Biology, Rutgers University-Camden, Camden, NJ 08102

[2]Department of Bioengineering, Stanford University, Stanford, CA 94305

[3]Department of Biochemistry and Biophysics, University of California San Francisco, San Francisco, CA 94158

[4]Department of Microbiology and Immunology, Stanford University School of Medicine, Stanford, CA 94305

[5]Chan Zuckerberg Biohub, San Francisco, CA 94158

[6]Biology Department, Rutgers University-Camden, Camden, NJ 08102

Correspondence:

Eric A. Klein

eric.a.klein@rutgers.edu

(856) 225-6335

24 Keywords: transpeptidase, stalk biosynthesis, LD crosslinks, LD transpeptidases, lysozyme, cell
25 shape

26

Summary

The diversity of cell shapes across the bacterial kingdom reflects evolutionary pressures that have produced physiologically important morphologies. While efforts have been made to understand the regulation of some prototypical cell morphologies such as that of rod-shaped *Escherichia coli*, little is known about most cell shapes. For *Caulobacter crescentus*, polar stalk synthesis is tied to its dimorphic life cycle, and stalk elongation is regulated by phosphate availability. Based on the previous observation that *C. crescentus* stalks are lysozyme-resistant, we compared the composition of the peptidoglycan cell wall of stalks and cell bodies and identified key differences in peptidoglycan crosslinking. Cell-body peptidoglycan contained primarily DD-crosslinks between *meso*-diaminopimelic acid and D-alanine residues, whereas stalk peptidoglycan had more LD-transpeptidation (*meso*-diaminopimelic acid-*meso*-diaminopimelic acid), mediated by LdtD. We determined that *ldtD* is dispensable for stalk elongation; rather, stalk LD-transpeptidation reflects an aging process associated with low peptidoglycan turnover in the stalk. We also found that lysozyme resistance is a structural consequence of LD-crosslinking. Despite no obvious selection pressure for LD-crosslinking or lysozyme resistance in *C. crescentus*, the correlation between these two properties was maintained in other organisms, suggesting that DAP-DAP crosslinking may be a general mechanism for regulating bacterial sensitivity to lysozyme.

Introduction

The bacterial kingdom contains species with a diverse array of morphologies, virtually all of which are determined by the peptidoglycan cell wall. Among the best-studied unusual morphologies are the stalks of the Alphaproteobacteria of the Caulobacteraceae family. The stalk is a unipolar extension of the cell envelope formed in a cell cycle-dependent manner in the model organism *Caulobacter crescentus*. The dimorphic life cycle of *C. crescentus* produces one motile (swarmer) cell and one adherent (stalked) cell upon each cell division (Stove Poindexter and Cohen-Bazire, 1964). The swarmer cell has a polar flagellum and pili, and is non-replicative. To enable cell division, the swarmer initiates a differentiation program in which it sheds its flagellum and, at the same pole, produces an adhesive holdfast (Tsang *et al.*, 2006). After the holdfast is secreted, the stalk forms and elongates from the holdfast pole, thereby causing the holdfast to be pushed away from the cell body and localized to the tip of the stalk. During cell division, a new flagellum is synthesized at the pole opposite the stalk. As a result, following cytokinesis, the stalked cell maintains its stalk and immediately reenters the cell cycle, while the swarmer daughter cell is flagellated and enters a quiescent state from which it needs to emerge before synthesizing a new stalk and beginning a proliferative cycle. In addition to its regulation by the cell cycle, stalk elongation is dramatically induced during phosphate limitation (Gonin *et al.*, 2000).

Since the stalk elongates upon phosphate limitation, one hypothesis is that the stalk acts as a "nutrient antenna" (Ireland *et al.*, 2002). Under diffusive conditions, nutrient uptake is proportional to cell length; therefore, having a long, thin appendage would be optimal for maximizing cell length while minimizing surface area (Wagner *et al.*, 2006). An alternative hypothesis is that by adhering to surfaces via the holdfast at the stalk tip, stalk elongation can

elevate *C. crescentus* cells off the surface to gain access to convective fluid flow, thereby increasing nutrient availability (Klein *et al.*, 2013).

Despite these hypotheses for the physiological role of stalk elongation, the molecular mechanisms of stalk synthesis remain unknown. This knowledge gap is due, in part, to uncertainty regarding the chemical composition of the stalk. Initial studies comparing the peptidoglycan of *C. crescentus* stalks and cell bodies were contradictory; their findings differed regarding the relative molar ratios of the amino acids alanine, diaminopimelic acid (DAP), and glutamic acid as well as between the glycan sugars *N*-acetylglucosamine (NAG) and *N*-acetylmuramic acid (NAM) (Fujiki *et al.*, 1976, Goodwin and Shedlarski, 1975, Poindexter and Hagenzieker, 1982). Despite these contradictory findings, physiological evidence supports the hypothesis that stalk peptidoglycan is somehow distinct from cell-body peptidoglycan. Treatment of *C. crescentus* cells with lysozyme to induce spheroplast formation leads to a peculiar "lollipop" morphology in which the cell body swells while the stalk retains its shape (Schmidt and Stanier, 1966), suggesting that stalk peptidoglycan may be more resistant to lysozyme-mediated degradation than cell-body peptidoglycan due to modifications in peptidoglycan composition.

The identification of enzymatic machinery directly responsible for stalk elongation has also been challenging. Peptidoglycan synthesis is mediated by a family of mono- and bi-functional penicillin-binding proteins (PBPs) that have glycosyltransferase and/or transpeptidase activities. Given the presence of peptidoglycan within the stalk (Schlimpert *et al.*, 2012), one or more of the PBPs is likely required for stalk elongation. Two recent studies reported that systematic deletion of the *C. crescentus* bi-functional PBPs and the single monofunctional glycosyltransferase, either individually or in combination, did not prevent stalk formation in low-

phosphate conditions (Strobel *et al.*, 2014, Yakhnina and Gitai, 2013); any single PBP (except PbpZ) was sufficient for growth and stalk biogenesis. These data suggest that either the redundancy of this activity allows any PBP to synthesize stalk peptidoglycan, or, consistent with its potentially unique composition, there are yet unidentified enzymes involved in stalk peptidoglycan insertion.

To distinguish among these possibilities, in this study we determined that stalk peptidoglycan is resistant to digestion by several lytic, cell wall-degrading hydrolases, including lysozyme and an interbacterial peptidoglycan amidase toxin. Muropeptide analysis via high-performance liquid chromatography (HPLC) revealed that this resistance in the stalk is due to increased cell wall LD-crosslinks between *meso*-DAP residues on adjacent peptidoglycan peptide stems. Further, we identified LdtD as the LD-transpeptidase required for stalk LD-crosslinking.

Results

C. crescentus stalks and cell bodies have different sensitivities to wall-degrading enzymes

The previous finding that the creation of *C. crescentus* spheroplasts with lysozyme leads to swollen cell bodies, while the stalk remains relatively unaffected (Schmidt and Stanier, 1966) (Fig. 1A), is surprising because high-resolution cryo-electron micrographs appear to show that the peptidoglycan cell wall is continuous and uniform from the cell body through the stalk (Schlimpert et al., 2012). We hypothesized that this phenomenon could be explained by two mechanisms: 1) although lysozyme efficiently degrades stalk peptidoglycan, the stalk does not swell due to lower turgor pressure and/or reduced mechanical stress in the wall (compared to the cell body) because the stalk has a narrower radius than the cell body, or 2) stalk peptidoglycan is

insensitive to lysozyme degradation. To directly test these hypotheses, we uniformly labeled the peptidoglycan of *C. crescentus* cells expressing periplasmic RFP by growing cells in Hutner-Imidazole-Glucose-Glutamate (HIGG) minimal medium containing 1 μM phosphate (HIGG + 1 μM phosphate) for 48 h in the presence of the fluorescent D-amino acid hydroxy coumarin-carbonyl-amino-D-alanine (HADA) (Kuru *et al.*, 2012). Cells were permeabilized with chloroform-saturated Tris buffer to ensure that the peptidoglycan would be accessible for lysozyme degradation. We confirmed outer-membrane permeability by visualizing the release of periplasmic RFP (Fig. 1B). Exposed peptidoglycan was treated with 25 μg mL^{-1} lysozyme for 15 min at 37 °C and the digested cells were imaged with fluorescence microscopy. While cell bodies were entirely degraded, stalks retained HADA fluorescence (Fig. 1B), demonstrating that stalks are more resistant to lysozyme than cell bodies.

To gain insight into the underlying properties of the stalk that provide lysozyme resistance, we asked whether lytic peptidoglycan-degrading enzymes that target other bonds within the cell wall degrade stalk peptidoglycan. Type VI secretion (T6S) systems are used by some bacteria to attack and kill neighboring cells; multiple effectors of type VI secretion systems function by degrading peptidoglycan components, leading to cell lysis (Russell *et al.*, 2011). *Salmonella enterica* serovar Typhi T6S amidase effector 3 (Tae3) specifically hydrolyzes DD-crosslinks between *meso*-DAP and D-alanine on adjacent peptide stems (Russell *et al.*, 2012). As with lysozyme, treatment of permeabilized *C. crescentus* cells with Tae3 led to complete digestion of the cell body while leaving stalks intact (Fig. 1C), indicating a difference in Tae3 activity between the two compartments.

Stalk and cell-body cell walls have distinct compositions and affinities for peptidoglycan-binding proteins

One potential explanation for the difference in enzymatic sensitivity between the two regions of the cell is a difference in peptidoglycan composition. We hypothesized that such a difference alters the affinity of proteins that bind peptidoglycan. The *gp144* endolysin gene from *Pseudomonas aeruginosa* phage ϕKZ contains an N-terminal peptidoglycan binding domain (Briers *et al.*, 2007). We purified a KZ144-YFP fusion protein and labeled permeabilized *C. crescentus* cells with it. Strikingly, KZ144-YFP exclusively labeled cell-body peptidoglycan and not stalk peptidoglycan (Fig. 1D), suggesting that stalk peptidoglycan is distinct from that of the cell body.

To identify compositional differences between these two compartments, we compared the muropeptide content of *C. crescentus* cells grown in HIGG + 1 mM or 1 μM phosphate, conditions under which cells have short or long stalks, respectively (Schlimpert et al., 2012). Sacculi were purified and digested with mutanolysin prior to muropeptide analysis via HPLC (Experimental Methods). Overall, the muropeptide content was qualitatively similar under both growth conditions, with the exception of one major peak that was uniquely present under low phosphate (elongated stalk) conditions (Fig. 1E, Table 1). Given the specificity of Tae3 for DD-crosslink digestion (Fig. 1F), the inability of Tae3 to degrade *C. crescentus* stalks suggests that the stalk compartment is enriched in LD-crosslinks between *meso*-DAP residues on neighboring peptide stems. Electrospray ionization mass spectrometry (ESI-MS) analysis of the peak observed during phosphate limitation confirmed that it is an LD-crosslinked muropeptide dimer (D43LD) (Fig. S1; the muropeptide naming convention is described in the legend for Table 1).

Stalk-specific LD-transpeptidation increases during stalk elongation

To determine whether LD-crosslinks are uniquely present in the stalk, we separated stalks from cell bodies and collected sacculi for muropeptide analysis. For validation, stalks were purified via two complementary methods. First, we harvested stalks from strain YB2811 (a derivative of NY111d1 with a *pstS::miniTn5* insertion), which spontaneously sheds stalks into the medium (Ireland et al., 2002, Poindexter, 1978). Second, stalks were collected from wild-type cells by mechanically detaching the stalks (Experimental Methods) (Wagner et al., 2006). In each case, peaks corresponding to LD-transpeptidation only appeared in stalk fractions (Fig. 2, Table 2); the identified LD-peaks correspond to dimers D33LD and D43LD and trimers T443LD and T443NLD as determined by confirmation via mass spectrometry (Fig. S2) and by comparison to published chromatograms (Glauner, 1988). While the two stalk-isolation methods yielded similar results with respect to LD-crosslinks, we consistently observed an increase in the pentapeptide M5G in mechanically sheared stalk samples; the reason for this enrichment is unclear.

To identify candidate LD-transpeptidases in *C. crescentus*, we used RPS-Blast (Marchler-Bauer *et al.*, 2017) to search for proteins containing conserved LD-transpeptidase domains (NCBI CDD database: COG2989, COG3034, COG3786, Pfam03734, PRK10594) and identified two candidates. CCNA_01579 has homology to *E. coli* LdtD (26% identical, 42% similar; henceforth referred to as LdtD) and CCNA_03860 is homologous to *Streptomyces purpurogeneiscleroticus* YkuD (42% identical, 53% similar; henceforth referred to as YkuD). Both proteins contain the conserved active site histidine and cysteine residues (Fig. S3A) (Magnet *et al.*, 2007). Analysis of stalk muropeptides in the Δ*ldtD* strain confirmed that this enzyme is responsible for 91% of the LD-crosslinking (Fig. 3A and Table 2). By contrast,

183 deletion of *ykuD* either alone or in combination with *ldtD* did not reduce LD-crosslinking (Table
184 2). Complementation of the *ldtD* deletion by expressing xylose-inducible *ldtD* confirmed the role
185 of LdtD in the formation of LD-crosslinks (Fig. S3B-D). We note that in the Δ*ldtD* and
186 Δ*ldtD*Δ*ykuD* strains we detected low levels of LD-crosslinks, particularly D33D and T443DN
187 (Table 2), suggesting *C. crescentus* may express an additional, as yet unidentified, LD-
188 transpeptidase.

189 The expression of *ldtD*, as determined by qRT-PCR and fluorescence intensity of an
190 LdtD-mCherry fusion at its native promoter, was significantly higher during growth in low (1
191 μM) phosphate compared with high (1 mM) phosphate, consistent with the hypothesized role of
192 LdtD in stalk peptidoglycan crosslinking (Fig. 3B). Despite the restriction of LD-crosslinks to
193 the stalk compartment, LdtD-mCherry was broadly localized throughout the entire cell envelope
194 when expressed either from the inducible *xylX* locus or from the native chromosomal locus under
195 its endogenous promoter (Fig. 3C). The fluorescence intensity was approximately constant
196 throughout the cell body and stalk (Fig. S4A); we observed ~15% higher fluorescence in the cell
197 body, although that increase may be an optical artifact due to the larger volume of that
198 compartment. The muropeptide composition of the *ldtD*::*ldtD-mCherry* strain in HIGG + 1 μM
199 phosphate was comparable to that in wild-type cells (Fig. 3D), demonstrating that the fluorescent
200 protein fusion is functional. While LD-transpeptidation regulates stalk peptidoglycan
201 muropeptide composition, deletion of *ldtD* or *ykuD* either alone or in combination had no effect
202 on stalk elongation (Fig. S4B). None of the LD-transpeptidase mutants had a growth defect in
203 either high or low phosphate (Fig. S4C). Taken together, these data establish LdtD as the major
204 LD-transpeptidase during stalk synthesis.
205

LD-transpeptidation mediates lysozyme sensitivity and KZ144 binding

To confirm the relationship between stalk LD-crosslinking and lysozyme resistance, we labeled wild-type and Δ*ldtD* peptidoglycan with HADA, permeabilized the outer membrane, and treated cells with lysozyme. Abrogation of LD-transpeptidation increased the sensitivity of stalk peptidoglycan to lysozyme-mediated degradation (Fig. 4A). Similarly, deletion of *ldtD* enabled stalk labeling by the phage peptidoglycan-binding protein KZ144-YFP (Fig. 4B). We note that KZ144-YFP binding was not entirely uniform within the cell body, with decreased labeling at the non-stalked pole in both wild-type and Δ*ldtD* cells (Fig. S5). These data suggest that there may be local variations in PG composition along the cell body.

Since the stalk is ~20% the width of the cell body (Wagner and Brun, 2007), we also considered whether geometrical constraints could contribute to the subcellular specificity of KZ144-YFP binding. If so, we expected that binding of KZ144-YFP would not be affected in wider rod-shaped cells, and would not be generally correlated with LD-transpeptidation levels. To address these possibilities, we labeled the peptidoglycan of *Agrobacterium tumefaciens* and *Hyphomonas neptunium*. Although the average cell size of *A. tumefaciens* is similar to *C. crescentus*, the growing pole (as determined by the pole with narrower width (Cameron *et al.*, 2014)) in log-phase *A. tumefaciens* cells bound more KZ144-YFP than did the opposite pole in the same cells (Fig. 4C). Interestingly, at least one LD-transpeptidase in *A. tumefaciens* localizes to the growing cell pole (Cameron *et al.*, 2014); although the precise distribution of LD-crosslinks has not been determined, it is possible that they are asymmetrically localized along the cell length, which could contribute to the gradient of KZ144-YFP binding. *H. neptunium* forms a stalk that is morphologically similar to the *C. crescentus* stalk, but this organism does not form DAP-DAP crosslinks (Cserti *et al.*, 2017). KZ144-YFP efficiently labeled DD-crosslinked stalks

in *H. neptunium* (Fig. 4D), leading us to conclude that binding affinity is regulated by the mode of crosslinking rather than by peptidoglycan geometry.

LD-transpeptidation correlates with lysozyme sensitivity in Gram-negative bacteria

Since LD-crosslinks in the *C. crescentus* stalk provided protection from degradation by lysozyme, we hypothesized that the 3-3 mode of transpeptidation may regulate lysozyme sensitivity more generally. During log-phase growth, LD-crosslinks account for 3.5% of muropeptides in *E. coli* (Pisabarro *et al.*, 1985). The fraction of these crosslinks increases to 8.6% in deep stationary phase (Pisabarro et al., 1985). *A. tumefaciens* peptidoglycan is enriched with LD-crosslinks, containing ~23% DAP-DAP (Brown *et al.*, 2012). To assess the relationship between the percentage of LD-crosslinks and lysozyme sensitivity, we permeabilized log-phase and stationary-phase *E. coli* as well as log-phase *A. tumefaciens* with chloroform-saturated Tris buffer and digested them with lysozyme. The turbidity of the treated cells was measured over time by measuring OD_{600}. LD-crosslink-deficient log-phase *E. coli* cells were the most susceptible to lysozyme degradation (Fig. 5A, S6). By contrast, DAP-DAP-rich *A. tumefaciens* cells were highly resistant (Fig. 5A, S6). Additionally, we detected a strong correlation between the initial rate of lysozyme degradation (0-60 s) and LD-crosslink content (R^2=0.975, Fig. 5B), suggesting that lysozyme sensitivity may be generally linked to LD-crosslinking.

Discussion

Based on the observation that *C. crescentus* lysozyme-induced spheroplasts display an unusual "lollipop" morphology (Schmidt and Stanier, 1966), we investigated the chemical composition of stalk peptidoglycan to determine the underlying mechanism of lysozyme resistance in the stalk. The recent development of fluorescent D-amino acids that label peptidoglycan *in vivo* (Kuru et al., 2012) enabled us to directly visualize the degradation of cell-body and stalk peptidoglycan by lysozyme (Fig. 1B) and the DD-amidase Tae3 (Fig. 1C), leading us to conclude that stalk peptidoglycan is more resistant to enzymatic digestion than cell-body peptidoglycan. Muropeptide analysis revealed that low-phosphate conditions promoting stalk elongation led to the accumulation of cell wall LD-crosslinks due to the activity of the LD-transpeptidase CCNA_01579 (LdtD) (Fig. 1E, 3A). LdtD specifically catalyzes transpeptidation in the stalk compartment (Fig. 2, 3A), and this particular mode of crosslinking confers resistance to lysozyme-mediated degradation within the stalk and in species with high levels of LD-crosslinks (Fig. 4A, 5A, B).

Regulation of LdtD activity in the stalk

Despite the enrichment of LD-crosslinks within the stalk, LdtD protein localization appears to be approximately uniform throughout the cell (Fig. 3C). Therefore, it is unclear how LdtD activity becomes restricted to the stalk compartment. One possibility is the availability of suitable substrates. Tetrapeptide DAP residues are the donor substrates for LD-crosslinking, and these tetrapeptide substrates generally are generated via the activity of DD-carboxypeptidases, which cleave between the fourth and fifth muropeptide residues. Comparing the muropeptide content of isolated stalks and cell bodies showed that stalks have elevated levels of tripeptides

and pentapeptides and reduced levels of tetrapeptides (Table 2), suggesting that carboxypeptidase activity is not responsible for generating additional substrate tetrapeptides. These data are consistent with the previously reported lack of carboxypeptidase activity in *C. crescentus* (Markiewicz *et al.*, 1983). Alternatively, DD-endopeptidases can cleave DD-crosslinks to create free tetrapeptides. While *C. crescentus* does not appear to have direct homologues to the known DD-endopeptidases PbpG, DacB, MepA, or EnvC, there are a large number of more distantly related peptidases, including an annotated AmpH homologue (CC_3489) that may serve this enzymatic function (Gonzalez-Leiza *et al.*, 2011). Finally, the high ratio of tetra-tetra dimers to tetra-tri dimers in the cell body fraction suggests that PBP enzymes prefer tetrapeptide substrates. In contrast, LdtD appears to make a significant number of tetra-tri crosslinks; therefore, the increased abundance of tripeptides in the stalk may serve as a preferred acceptor substrate for LdtD, although the underlying mechanism for accumulating tripeptides is unknown.

Function of LD-transpeptidation in the stalk

For the majority of bacterial species that have been investigated to date, the dominant mode of peptidoglycan crosslinking is DD-transpeptidation mediated by PBPs. In species that use a polar growth mechanism, such as those of the orders Actinomycetales (Lavollay *et al.*, 2011) and Rhizobiales (Brown et al., 2012), LD-crosslinks can constitute ~40-80% of the total crosslinks. In *A. tumefaciens*, the Ldt Atu0845 localizes to the growing pole, consistent with its hypothesized role in polar elongation (Cameron et al., 2014). Given that the Alphaproteobacteria *C. crescentus* and *A. tumefaciens* are in the same phylogenetic class, as well as the specific accumulation of LD-crosslinks in the stalk (Fig. 2), it was tempting to hypothesize that stalk

elongation represents a form of Ldt-driven polar growth. However, deletion of *ldtD* did not result in any stalk-elongation defect (Fig. S4B). Moreover, unlike Atu0845 (Cameron et al., 2014), LdtD-mCherry was uniformly distributed throughout the cell body and stalk envelope (Fig. 3C).

An alternative model for stalk Ldt activity arises from the pattern of LD-crosslinking in *E. coli*. DAP-DAP crosslinking increases during stationary phase (Pisabarro et al., 1985), when incorporation of new peptidoglycan material is dramatically reduced (Blasco *et al.*, 1988). Similarly, since the *C. crescentus* stalk is built by inserting new peptidoglycan material at its base at the cell pole (Hughes *et al.*, 2013), there appears to be a very low rate of new peptidoglycan insertion in the stalk relative to the cell body. Although the role of LD-transpeptidation in *E. coli* during stationary phase is unknown, *C. crescentus* LdtD may play a similar role in peptidoglycan maintenance in the stalk.

LD-transpeptidation increases lysozyme resistance

Typically, lysozyme resistance is attributed to one of several modifications of the glycan strands, including MurNac O-acetylation, GlcNac N-deacetylation, and MurNac O-glycolylation (reviewed in (Davis and Weiser, 2011)). While the *C. crescentus* genome does not contain any genes with obvious O-acetylation or O-glycolylation activity, it does encode two orthologs of *Streptococcus pneumoniae* GlcNac N-deacetylase *pgdA*; one of these genes, *hfsH*, regulates the adhesiveness of holdfast (Wan *et al.*, 2013). The role of the second ortholog, CCNA_02236, is unknown, leaving open the possibility that GlcNac N-deacetylation may play a role in regulating lysozyme resistance in *C. crescentus*.

Lysozyme digestion of *C. crescentus* stalks (Fig. 4A) as well as whole-cell peptidoglycan from *E. coli* and *A. tumefaciens* (Fig. 5A,B) suggests a relationship between the degree of LD-

316 transpeptidation and lysozyme sensitivity. This relationship is somewhat surprising: lysozyme
317 acts by hydrolyzing the NAM-NAG glycosidic bond on the glycan backbone, whereas LD-
318 crosslinks occur on the peptide stem. Computational models of peptidoglycan structure propose
319 several conformational differences between LD- and DD-crosslinks that may explain this
320 phenomenon (de Pedro and Cava, 2015). First, lack of the D-alanine residue linking the *meso*-
321 DAP molecules in the LD-crosslink may make the stem peptides more rigid, leading to a more
322 extended conformation and a greater distance between glycan strands. Second, DD-crosslinks
323 allow the formation of additional hydrogen bonds that can affect the favored orientation of the
324 NAG-NAM disaccharides in the glycan strand. The overall effect of LD-transpeptidation on
325 peptidoglycan conformation may explain the decreased activity and affinity of lysozyme as well
326 as those of the KZ144 peptidoglycan-binding domain.
327 Our analysis of *E. coli* and *A. tumefaciens* peptidoglycan lysozyme susceptibility
328 suggests that the relationship between LD-crosslinking and lysozyme insensitivity may be a
329 more general cellular property. In the context of bacterial pathogenesis, lysozyme is a significant
330 player in host defense. For example, in a mouse model of lung infection by *Klebsiella*
331 *pneumoniae*, lysozyme M knockout mice did not survive beyond 72 h post infection, whereas
332 25% of wild-type mice survived up to 120 h (Markart *et al.*, 2004). Transcriptomic analysis of *K.*
333 *pneumoniae* exposed to pulmonary surfactant showed that relative to controls, interaction with
334 lung secretions increased *ybiS* LD-transpeptidase expression (Willsey *et al.*, 2018). Upregulation
335 of *ybiS* expression may be part of a general envelope stress response, similar to the increase of *E.*
336 *coli ldtD* transcription during the Cpx envelope stress response (Bernal-Cabas *et al.*, 2015);
337 alternatively, it may be a specific program for modulating peptidoglycan composition to avoid
338 killing by the host lysozyme defense. Increasing the proportion of LD-crosslinks also increases

bacterial pathogenicity by enhancing resistance against beta-lactam antibiotics (Cremniter *et al.*, 2006, Gupta *et al.*, 2010, Hugonnet *et al.*, 2016). In *E. coli*, inhibition of PBPs by beta-lactams blocks DD-transpeptidation, leading to peptidoglycan instability and cell death; this phenotype is suppressed by overexpression of LdtD and production of (p)ppGpp by the stringent response (Hugonnet et al., 2016).

Robust maintenance of cell shape may benefit from redundancy in peptidoglycan-modifying enzymes

For most rod-shaped bacteria, including *C. crescentus*, DD-transpeptidation is the dominant form of peptidoglycan crosslinking. Since peptidoglycan organization and stability are critical for cellular integrity, it is perhaps not surprising that many of these organisms encode a highly redundant set of high-molecular weight PBPs with DD-transpeptidase activity. For example, *E. coli*, *C. crescentus*, and *Bacillus subtilis* encode five, seven, and 10 high-molecular weight PBPs, respectively (Blattner *et al.*, 1997, Kunst *et al.*, 1997, Nierman *et al.*, 2001). Redundancy among the bifunctional class A PBPs allows many of these genes to be deleted singly or in combination without losing viability; however, deletion of all members of this enzyme class is lethal (Denome *et al.*, 1999, Strobel et al., 2014, Yakhnina and Gitai, 2013). In contrast, these species have relatively low abundances of LD-crosslinks, and LD-transpeptidase activity is dispensable. *E. coli* and *C. crescentus* encode six and two Ldt enzymes, respectively; deletion of these genes, even in combination, does not yield any observable phenotype under normal growth conditions (Sanders and Pavelka, 2013) (Fig. S4B-D). The function of LD-transpeptidases in these organisms remains largely unknown; however, they may have a role in optimizing peptidoglycan architecture or responding to particular environmental stresses. Two of

362 the *E. coli* Ldt enzymes are responsible for DAP-DAP crosslinking (Magnet *et al.*, 2008), while
363 several others link the peptidoglycan to Braun's lipoprotein (Magnet et al., 2007). While *C.*
364 *crescentus* does not contain Braun's lipoprotein, our observation that deletion of *ykuD* has no
365 effect on PG composition suggests that there may be an alternative substrate for this enzyme as
366 well.

367 In contrast, LD-transpeptidases of Rhizobiales and Actinomycetales species that elongate
368 via polar growth may take on a more significant role. *Mycobacterium tuberculosis* has five Ldt
369 proteins, and the loss of just two isoforms (LdtMt1 and LdtMt2) causes defects in cell shape,
370 growth, and virulence (Schoonmaker *et al.*, 2014). Most species of Rhizobiales, including *A.*
371 *tumefaciens*, have 12-16 Ldt genes, leading to extensive redundancy (Cameron *et al.*, 2015).
372 Thus, it appears that over a wide spectrum of organisms with varying growth modes, there is a
373 selective pressure to maintain redundancy in the elongation machinery. This insight may be
374 useful for predicting the elongation modes of species using metagenomic data based on their
375 complement of PBP and Ldt genes, thereby providing a framework for understanding the link
376 between cell growth and environmental, ecological, and pathogenicity factors.
377

Experimental Methods

Bacterial strains, plasmids, and growth conditions

The strains, plasmids, and primers used in this study are described in Tables S1, S2, and S3, respectively. *C. crescentus* wild-type strain NA1000 and its derivatives were routinely cultured at 30 °C in peptone yeast extract medium (Poindexter, 1964). In experiments where phosphate levels were varied, *C. crescentus* strains were grown in Hutner-Imidazole-Glucose-Glutamate (HIGG) minimal medium supplemented with 1 or 1000 µM phosphate (Poindexter, 1978). *E. coli* strains were grown at 37 °C in liquid lysogeny broth (LB). *A. tumefaciens* strain C58 (kind gift from Zemer Gitai, Princeton University) was grown at 30 °C in peptone yeast extract medium. *H. neptunium* strain 14-15 (ATCC) was grown at room temperature in Difco Marine Broth 2216. When necessary, antibiotics were added at the following concentrations: kanamycin, 30 µg mL^{-1} in broth and 50 µg mL^{-1} in agar for *E. coli* and 5 µg mL^{-1} in broth and 25 µg mL^{-1} in agar for *C. crescentus*; tetracycline, 12 µg mL^{-1} in broth and 12 µg mL^{-1} in agar for *E. coli* and 1 µg mL^{-1} in broth and 2 µg mL^{-1} in agar for *C. crescentus*; chloramphenicol, 1 µg mL^{-1} in broth and 1 µg mL^{-1} in agar for *C. crescentus*; gentamicin, 15 µg mL^{-1} in broth and 20 µg mL^{-1} in agar for *E. coli* and 5 µg mL^{-1} in broth and 0.5 µg mL^{-1} in agar for *C. crescentus*. Where noted, gene expression was induced in *C. crescentus* with 0.3% (w/v) xylose. Peptidoglycan was fluorescently labeled by adding 0.25 mM HADA (purchased under a Material Transfer Agreement from Indiana University) to the growth medium (Kuru et al., 2012).

Protein purification

KZ144-YFP was cloned into pET28a (Novagen) and expressed in BL21(DE3) cells (New England Biolabs) to produce strain EK313. EK313 was grown overnight in LB, diluted 1:60 into

20 mL LB, and grown to OD_{600} 0.6. Expression was induced for 4 h with 1 mM IPTG. Five milliliters of cells were collected via centrifugation (10 min, 3,800 x *g*, 4 °C), and protein was purified using the Qiagen Ni-NTA Spin Kit in accordance with the manufacturer's protocol. Tae3 was cloned into the pET29b+ vector (Novagen) and expressed in Shuffle Express T7 lysY cells (New England Biolabs). Proteins were purified to homogeneity using previously reported methods (Russell et al., 2012), except that in all steps no reducing agents or lysozyme were used.

Fluorescence microscopy and image analysis

Cells were spotted onto 1% agarose pads. Fluorescence microscopy was performed on a Nikon Ti-E inverted microscope equipped with a Prior Lumen 220PRO illumination system, CFI Plan Apochromat 100X oil immersion objective (NA 1.45, WD 0.13 mm), Zyla sCMOS 5.5-megapixel camera (Andor), and NIS Elements v, 4.20.01 for image acquisition. Stalk lengths and envelope fluorescence profiles were measured using ImageJ v. 1.48q (NIH). Cell body length, total cell fluorescence, and centerline fluorescence were quantified using *Morphometrics* (Ursell et al., 2017) and Matlab v. R2015b.

Transmission electron microscopy

Droplets of cell suspensions were placed on a strip of Parafilm. Formvar-coated copper grids (Electron Microscopy Sciences) were floated on top of the cell suspensions for 1 min. The grids were washed twice with water and then negatively stained with 1% uranyl acetate (Electron Microscopy Sciences). Following an additional wash with water, the grids were imaged on a Zeiss EM902 transmission electron microscope.

Cell permeabilization and labeling

For experiments requiring enzymatic treatment of peptidoglycan for microscopy and analysis, the outer membrane was removed via chloroform permeabilization. Chloroform-saturated Tris buffer was prepared by mixing 50 mM Tris [pH 7.4] with chloroform (70:30) and shaking the mixture at room temperature for 30 min. Cells to be permeabilized were collected via centrifugation (2 min at 6,000 x *g*, 4 °C) and resuspended in an equal volume of the aqueous phase of the chloroform-saturated Tris buffer. Resuspended cells were rocked for 45 min at room temperature and then washed twice in 50 mM Tris [pH 7.4] (via centrifugation for 10 min at 5,000 x *g*) to remove residual chloroform. Cells were labeled with purified KZ144-YFP (0.1-0.2 mg mL^{-1}; purification described above) for 5 min at room temperature and washed twice with 50 mM Tris [pH 7.4].

Muropeptide purification

For whole *C. crescentus* cells, we started with 500-ml cultures grown in either high-phosphate (1 mM) or low-phosphate (1 µM) HIGG growth media. To mechanically detach stalks from cell bodies, cells from 3 L cultures were sheared in a standard kitchen blender for 1 min at maximum speed. For mechanically sheared cells and the stalk-shedding YB2811 strain, cell bodies were purified via low-speed centrifugation (10 min at 8,000 x *g*, 4 °C); excess cell bodies were removed via 2-3 spins for 10 min at 10,000 x *g*. The removal of cell bodies was assessed by phase microscopy. Subsequently, pure stalks were harvested from the washed supernatant (1 h centrifugation at 47,056 x *g*). Peptidoglycan muropeptides were purified from *C. crescentus* as previously described (Desmarais *et al.*, 2014) and separated on a reversed-phase C18 column (Thermo Scientific; 250 x 4.6-mm column, 3-µm particle size) held at 55 °C. The LC solvent

system consisted of 50 mM sodium phosphate [pH 4.35] with 0.4% sodium azide (solvent A) and 75 mM sodium phosphate, pH 4.95 + 15% (v/v) methanol (solvent B). The solvent flow rate was 0.5 mL min^{-1} and a linear gradient to 100% solvent B was performed over 135 min. Muropeptide elution was monitored at 205 nm and sample fractions were collected at time points as indicated. Collected fractions were dried via vacuum centrifugation and analyzed by ESI-MS at the Rutgers Biological Mass Spectrometry Facility. Major peaks were labeled based on previous analysis of *C. crescentus* muropeptides (Takacs *et al.*, 2010). LD-crosslinks were labeled based on previous analysis of *E. coli* muropeptides (Glauner, 1988) and confirmed by LC/MS. Muropeptide abundances were measured using *Chromanalysis* v. 1.0 (Desmarais *et al.*, 2015).

Quantitative RT-PCR (qRT-PCR)

Cells (0.5-5 mL) were collected via centrifugation (10 min, 3,800 x *g*, 4 °C) and resuspended in Bacterial RNA Protect (Qiagen) in accordance with the manufacturer's protocol. RNA was purified using the RNeasy Mini Kit (Qiagen) and contaminating DNA was removed via on-column digestion (Qiagen). Purified RNA (5 ng μL^{-1}) was reverse-transcribed using the ABI High Capacity cDNA Reverse Transcription kit. Control samples did not contain reverse transcriptase to assess the level of DNA contamination. cDNA was amplified using Power SYBR Green Master Mix (Thermo Scientific) and analyzed on a Quantstudio 6 instrument (Thermo Scientific). Quantification of qRT-PCR data was performed using the ΔΔCt method (Livak and Schmittgen, 2001) with *rpoD* as the endogenous control.

Cell growth assay

Cells were grown overnight in the media to be used for growth analysis. The optical density at 660 nm (OD_{660}) was normalized to 0.03 for each strain. Cell growth was assessed by measuring OD_{660} in 96-well format using a CLARIOstar plate reader (BMG Labtech) incubated at 30 °C with shaking.

In vitro lysozyme sensitivity assay

Cells were chloroform-permeabilized as described above. The OD_{600} for each sample was normalized to 0.08 by measuring the absorbance of a 15-µL sample in a 384-well plate using a CLARIOstar plate reader. To measure the rate of digestion, lysozyme was added to 15-µL cell suspensions at a final concentration of 1 µg mL^{-1} and OD_{600} was measured at 30-s intervals over 15 min without shaking. A linear regression to the first 60 s of data was used to determine the initial degradation rate.

Acknowledgments

We thank Dr. Haiyan Zheng and the Rutgers Biological Mass Spectrometry Facility for their assistance in acquiring mass spectrometry data. Funding was provided by NSF CAREER Award MCB-1149328, the Stanford Center for Systems Biology under Grant P50-GM107615, and the Allen Discovery Center at Stanford on Systems Modeling of Infection (to K.C.H); the UCSF Program for Breakthrough Biomedical Research (to S.C.); and NSF CAREER Award MCB-1553004 (to E.A.K.). S.C. and K.C.H. are Chan Zuckerberg Investigators.

Author Contributions

GS, SC, KCH, and EAK contributed to the conception and design of the project. GS, AM, AR, SC, KCH, and EAK contributed to the acquisition, analysis, and/or interpretation of the data. EAK wrote and GS, SC, and KCH edited the manuscript. All authors reviewed the manuscript prior to submission.

References

Bernal-Cabas, M., Ayala, J. A. and Raivio, T. L. (2015) The Cpx envelope stress response modifies peptidoglycan cross-linking via the L,D-transpeptidase LdtD and the novel protein YgaU. *J Bacteriol* **197**: 603-614.

Blasco, B., Pisabarro, A. G. and de Pedro, M. A. (1988) Peptidoglycan biosynthesis in stationary-phase cells of *Escherichia coli*. *J Bacteriol* **170**: 5224-5228.

Blattner, F. R., Plunkett, G., 3rd, Bloch, C. A., Perna, N. T., Burland, V., Riley, M., Collado-Vides, J., Glasner, J. D., Rode, C. K., Mayhew, G. F., Gregor, J., Davis, N. W., Kirkpatrick, H. A., Goeden, M. A., Rose, D. J., Mau, B. and Shao, Y. (1997) The complete genome sequence of *Escherichia coli* K-12. *Science* **277**: 1453-1462.

Briers, Y., Volckaert, G., Cornelissen, A., Lagaert, S., Michiels, C. W., Hertveldt, K. and Lavigne, R. (2007) Muralytic activity and modular structure of the endolysins of *Pseudomonas aeruginosa* bacteriophages phiKZ and EL. *Mol Microbiol* **65**: 1334-1344.

Brown, P. J., de Pedro, M. A., Kysela, D. T., Van der Henst, C., Kim, J., De Bolle, X., Fuqua, C. and Brun, Y. V. (2012) Polar growth in the Alphaproteobacterial order Rhizobiales. *Proc Natl Acad Sci U S A* **109**: 1697-1701.

Cameron, T. A., Anderson-Furgeson, J., Zupan, J. R., Zik, J. J. and Zambryski, P. C. (2014) Peptidoglycan synthesis machinery in *Agrobacterium tumefaciens* during unipolar growth and cell division. *MBio* **5**: e01219-01214.

Cameron, T. A., Zupan, J. R. and Zambryski, P. C. (2015) The essential features and modes of bacterial polar growth. *Trends Microbiol* **23**: 347-353.

Cremniter, J., Mainardi, J. L., Josseaume, N., Quincampoix, J. C., Dubost, L., Hugonnet, J. E., Marie, A., Gutmann, L., Rice, L. B. and Arthur, M. (2006) Novel mechanism of

resistance to glycopeptide antibiotics in *Enterococcus faecium*. *J Biol Chem* **281**: 32254-32262.

Cserti, E., Rosskopf, S., Chang, Y. W., Eisheuer, S., Selter, L., Shi, J., Regh, C., Koert, U., Jensen, G. J. and Thanbichler, M. (2017) Dynamics of the peptidoglycan biosynthetic machinery in the stalked budding bacterium *Hyphomonas neptunium*. *Mol Microbiol* **103**: 875-895.

Davis, K. M. and Weiser, J. N. (2011) Modifications to the peptidoglycan backbone help bacteria to establish infection. *Infect Immun* **79**: 562-570.

de Pedro, M. A. and Cava, F. (2015) Structural constraints and dynamics of bacterial cell wall architecture. *Front Microbiol* **6**: 449.

Denome, S. A., Elf, P. K., Henderson, T. A., Nelson, D. E. and Young, K. D. (1999) *Escherichia coli* mutants lacking all possible combinations of eight penicillin binding proteins: viability, characteristics, and implications for peptidoglycan synthesis. *J Bacteriol* **181**: 3981-3993.

Desmarais, S. M., Cava, F., de Pedro, M. A. and Huang, K. C. (2014) Isolation and preparation of bacterial cell walls for compositional analysis by ultra performance liquid chromatography. *J Vis Exp*: e51183.

Desmarais, S. M., Tropini, C., Miguel, A., Cava, F., Monds, R. D., de Pedro, M. A. and Huang, K. C. (2015) High-throughput, highly sensitive analyses of bacterial morphogenesis using ultra performance liquid chromatography. *J Biol Chem* **290**: 31090-31100.

Fujiki, K., Fukuda, A. and Okada, Y. (1976) Amino acid composition of peptidoglycan in *Caulobacter crescentus*. *J Biochem* **80**: 1453-1455.

542 Glauner, B. (1988) Separation and quantification of muropeptides with high-performance liquid
543 chromatography. *Anal Biochem* **172**: 451-464.
544 Gonin, M., Quardokus, E. M., O'Donnol, D., Maddock, J. and Brun, Y. V. (2000) Regulation of
545 stalk elongation by phosphate in *Caulobacter crescentus*. *J. Bacteriol.* **182**: 337-347.
546 Gonzalez-Leiza, S. M., de Pedro, M. A. and Ayala, J. A. (2011) AmpH, a bifunctional DD-
547 endopeptidase and DD-carboxypeptidase of *Escherichia coli*. *J Bacteriol* **193**: 6887-
548 6894.
549 Goodwin, S. D. and Shedlarski, J. G., Jr. (1975) Purification of cell wall peptidoglycan of the
550 dimorphic bacterium *Caulobacter crescentus*. *Arch Biochem Biophys* **170**: 23-36.
551 Gupta, R., Lavollay, M., Mainardi, J. L., Arthur, M., Bishai, W. R. and Lamichhane, G. (2010)
552 The *Mycobacterium tuberculosis* protein LdtMt2 is a nonclassical transpeptidase required
553 for virulence and resistance to amoxicillin. *Nat Med* **16**: 466-469.
554 Hughes, H. V., Lisher, J. P., Hardy, G. G., Kysela, D. T., Arnold, R. J., Giedroc, D. P. and Brun,
555 Y. V. (2013) Co-ordinate synthesis and protein localization in a bacterial organelle by the
556 action of a penicillin-binding-protein. *Mol Microbiol* **90**: 1162-1177.
557 Hugonnet, J. E., Mengin-Lecreulx, D., Monton, A., den Blaauwen, T., Carbonnelle, E., Veckerle,
558 C., Brun, Y. V., van Nieuwenhze, M., Bouchier, C., Tu, K., Rice, L. B. and Arthur, M.
559 (2016) Factors essential for L,D-transpeptidase-mediated peptidoglycan cross-linking and
560 beta-lactam resistance in *Escherichia coli*. *Elife* **5**.
561 Ireland, M. M., Karty, J. A., Quardokus, E. M., Reilly, J. P. and Brun, Y. V. (2002) Proteomic
562 analysis of the *Caulobacter crescentus* stalk indicates competence for nutrient uptake.
563 *Mol Microbiol* **45**: 1029-1041.

564 Klein, E. A., Schlimpert, S., Hughes, V., Brun, Y. V., Thanbichler, M. and Gitai, Z. (2013)
565 Physiological role of stalk lengthening in *Caulobacter crescentus*. *Commun Integr Biol* **6**:
566 e24561.
567 Kunst, F., Ogasawara, N., Moszer, I., Albertini, A. M., Alloni, G., Azevedo, V., Bertero, M. G.,
568 Bessieres, P., Bolotin, A., Borchert, S., Borriss, R., Boursier, L., Brans, A., Braun, M.,
569 Brignell, S. C., Bron, S., Brouillet, S., Bruschi, C. V., Caldwell, B., Capuano, V., Carter,
570 N. M., Choi, S. K., Cordani, J. J., Connerton, I. F., Cummings, N. J., Daniel, R. A.,
571 Denziot, F., Devine, K. M., Dusterhoft, A., Ehrlich, S. D., Emmerson, P. T., Entian, K.
572 D., Errington, J., Fabret, C., Ferrari, E., Foulger, D., Fritz, C., Fujita, M., Fujita, Y.,
573 Fuma, S., Galizzi, A., Galleron, N., Ghim, S. Y., Glaser, P., Goffeau, A., Golightly, E. J.,
574 Grandi, G., Guiseppi, G., Guy, B. J., Haga, K., Haiech, J., Harwood, C. R., Henaut, A.,
575 Hilbert, H., Holsappel, S., Hosono, S., Hullo, M. F., Itaya, M., Jones, L., Joris, B.,
576 Karamata, D., Kasahara, Y., Klaerr-Blanchard, M., Klein, C., Kobayashi, Y., Koetter, P.,
577 Koningstein, G., Krogh, S., Kumano, M., Kurita, K., Lapidus, A., Lardinois, S., Lauber,
578 J., Lazarevic, V., Lee, S. M., Levine, A., Liu, H., Masuda, S., Mauel, C., Medigue, C.,
579 Medina, N., Mellado, R. P., Mizuno, M., Moestl, D., Nakai, S., Noback, M., Noone, D.,
580 O'Reilly, M., Ogawa, K., Ogiwara, A., Oudega, B., Park, S. H., Parro, V., Pohl, T. M.,
581 Portelle, D., Porwollik, S., Prescott, A. M., Presecan, E., Pujic, P., Purnelle, B., et al.
582 (1997) The complete genome sequence of the gram-positive bacterium *Bacillus subtilis*.
583 *Nature* **390**: 249-256.
584 Kuru, E., Hughes, H. V., Brown, P. J., Hall, E., Tekkam, S., Cava, F., de Pedro, M. A., Brun, Y.
585 V. and VanNieuwenhze, M. S. (2012) In situ probing of newly synthesized peptidoglycan

in live bacteria with fluorescent D-amino acids. *Angew Chem Int Ed Engl* **51**: 12519-12523.

Lavollay, M., Fourgeaud, M., Herrmann, J. L., Dubost, L., Marie, A., Gutmann, L., Arthur, M. and Mainardi, J. L. (2011) The peptidoglycan of M*ycobacterium abscessus* is predominantly cross-linked by L,D-transpeptidases. *J Bacteriol* **193**: 778-782.

Livak, K. J. and Schmittgen, T. D. (2001) Analysis of relative gene expression data using real-time quantitative PCR and the 2(-Delta Delta C(T)) Method. *Methods* **25**: 402-408.

Magnet, S., Bellais, S., Dubost, L., Fourgeaud, M., Mainardi, J. L., Petit-Frere, S., Marie, A., Mengin-Lecreulx, D., Arthur, M. and Gutmann, L. (2007) Identification of the L,D-transpeptidases responsible for attachment of the Braun lipoprotein to *Escherichia coli* peptidoglycan. *J Bacteriol* **189**: 3927-3931.

Magnet, S., Dubost, L., Marie, A., Arthur, M. and Gutmann, L. (2008) Identification of the L,D-transpeptidases for peptidoglycan cross-linking in *Escherichia coli*. *J Bacteriol* **190**: 4782-4785.

Marchler-Bauer, A., Bo, Y., Han, L., He, J., Lanczycki, C. J., Lu, S., Chitsaz, F., Derbyshire, M. K., Geer, R. C., Gonzales, N. R., Gwadz, M., Hurwitz, D. I., Lu, F., Marchler, G. H., Song, J. S., Thanki, N., Wang, Z., Yamashita, R. A., Zhang, D., Zheng, C., Geer, L. Y. and Bryant, S. H. (2017) CDD/SPARCLE: functional classification of proteins via subfamily domain architectures. *Nucleic Acids Res* **45**: D200-D203.

Markart, P., Korfhagen, T. R., Weaver, T. E. and Akinbi, H. T. (2004) Mouse lysozyme M is important in pulmonary host defense against *Klebsiella pneumoniae* infection. *Am J Respir Crit Care Med* **169**: 454-458.

608 Markiewicz, Z., Glauner, B. and Schwarz, U. (1983) Murein structure and lack of DD- and LD-
609 carboxypeptidase activities in *Caulobacter crescentus*. *J Bacteriol* **156**: 649-655.
610 Nierman, W. C., Feldblyum, T. V., Laub, M. T., Paulsen, I. T., Nelson, K. E., Eisen, J. A.,
611 Heidelberg, J. F., Alley, M. R., Ohta, N., Maddock, J. R., Potocka, I., Nelson, W. C.,
612 Newton, A., Stephens, C., Phadke, N. D., Ely, B., DeBoy, R. T., Dodson, R. J., Durkin,
613 A. S., Gwinn, M. L., Haft, D. H., Kolonay, J. F., Smit, J., Craven, M. B., Khouri, H.,
614 Shetty, J., Berry, K., Utterback, T., Tran, K., Wolf, A., Vamathevan, J., Ermolaeva, M.,
615 White, O., Salzberg, S. L., Venter, J. C., Shapiro, L. and Fraser, C. M. (2001) Complete
616 genome sequence of *Caulobacter crescentus*. *Proc Natl Acad Sci U S A* **98**: 4136-4141.
617 Pisabarro, A. G., de Pedro, M. A. and Vazquez, D. (1985) Structural modifications in the
618 peptidoglycan of *Escherichia coli* associated with changes in the state of growth of the
619 culture. *J Bacteriol* **161**: 238-242.
620 Poindexter, J. S. (1964) Biological properties and classification of the Caulobacter group.
621 *Bacteriol Rev* **28**: 231-295.
622 Poindexter, J. S. (1978) Selection for nonbuoyant morphological mutants of *Caulobacter*
623 *crescentus*. *J Bacteriol* **135**: 1141-1145.
624 Poindexter, J. S. and Hagenzieker, J. G. (1982) Novel peptidoglycans in Caulobacter and
625 Asticcacaulis spp. *J Bacteriol* **150**: 332-347.
626 Russell, A. B., Hood, R. D., Bui, N. K., LeRoux, M., Vollmer, W. and Mougous, J. D. (2011)
627 Type VI secretion delivers bacteriolytic effectors to target cells. *Nature* **475**: 343-347.
628 Russell, A. B., Singh, P., Brittnacher, M., Bui, N. K., Hood, R. D., Carl, M. A., Agnello, D. M.,
629 Schwarz, S., Goodlett, D. R., Vollmer, W. and Mougous, J. D. (2012) A widespread

bacterial type VI secretion effector superfamily identified using a heuristic approach. *Cell Host Microbe* **11**: 538-549.

Sanders, A. N. and Pavelka, M. S. (2013) Phenotypic analysis of *Eschericia coli* mutants lacking L,D-transpeptidases. *Microbiology* **159**: 1842-1852.

Schlimpert, S., Klein, E. A., Briegel, A., Hughes, V., Kahnt, J., Bolte, K., Maier, U. G., Brun, Y. V., Jensen, G. J., Gitai, Z. and Thanbichler, M. (2012) General protein diffusion barriers create compartments within bacterial cells. *Cell* **151**: 1270-1282.

Schmidt, J. M. and Stanier, R. Y. (1966) The development of cellular stalks in bacteria. *The Journal of cell biology* **28**: 423.

Schoonmaker, M. K., Bishai, W. R. and Lamichhane, G. (2014) Nonclassical transpeptidases of *Mycobacterium tuberculosis* alter cell size, morphology, the cytosolic matrix, protein localization, virulence, and resistance to beta-lactams. *J Bacteriol* **196**: 1394-1402.

Stove Poindexter, J. L. and Cohen-Bazire, G. (1964) The fine structure of stalked bacteria belonging to the family Caulobacteraceae. *Journal of Cell Biology* **23**: 587-607.

Strobel, W., Moll, A., Kiekebusch, D., Klein, K. E. and Thanbichler, M. (2014) Function and localization dynamics of bifunctional penicillin-binding proteins in *Caulobacter crescentus*. *J Bacteriol* **196**: 1627-1639.

Takacs, C. N., Poggio, S., Charbon, G., Pucheault, M., Vollmer, W. and Jacobs-Wagner, C. (2010) MreB drives de novo rod morphogenesis in *Caulobacter crescentus* via remodeling of the cell wall. *J Bacteriol* **192**: 1671-1684.

Tsang, P. H., Li, G., Brun, Y. V., Freund, L. B. and Tang, J. X. (2006) Adhesion of single bacterial cells in the micronewton range. *PNAS* **103**: 5764-5768.

652 Ursell, T., Lee, T. K., Shiomi, D., Shi, H., Tropini, C., Monds, R. D., Colavin, A., Billings, G.,
653 Bhaya-Grossman, I., Broxton, M., Huang, B. E., Niki, H. and Huang, K. C. (2017) Rapid,
654 precise quantification of bacterial cellular dimensions across a genomic-scale knockout
655 library. *BMC Biol* **15**: 17.
656 Wagner, J. K. and Brun, Y. V. (2007) Out on a limb: how the *Caulobacter* stalk can boost the
657 study of bacterial cell shape. *Mol Microbiol* **64**: 28-33.
658 Wagner, J. K., Setayeshgar, S., Sharon, L. A., Reilly, J. P. and Brun, Y. V. (2006) A nutrient
659 uptake role for bacterial cell envelope extensions. *Proc Natl Acad Sci U S A* **103**: 11772-
660 11777.
661 Wan, Z., Brown, P. J., Elliott, E. N. and Brun, Y. V. (2013) The adhesive and cohesive
662 properties of a bacterial polysaccharide adhesin are modulated by a deacetylase. *Mol*
663 *Microbiol* **88**: 486-500.
664 Willsey, G. G., Ventrone, S., Schutz, K. C., Wallace, A. M., Ribis, J. W., Suratt, B. T. and
665 Wargo, M. J. (2018) Pulmonary surfactant promotes virulence gene expression and
666 biofilm formation in *Klebsiella pneumoniae*. *Infect Immun* **86**.
667 Yakhnina, A. A. and Gitai, Z. (2013) Diverse functions for six glycosyltransferases in
668 *Caulobacter crescentus* cell wall assembly. *J Bacteriol* **195**: 4527-4535.
669
670
671

672 **Table 1. Muropeptide analyses of *C. crescentus* under varying phosphate concentrations.**

673 Muropeptides were purified from NA1000 cells grown in 1 mM or 1 μM phosphate and analyzed
674 by HPLC (Methods). Peaks were labeled and quantified using *Chromanalysis* (Desmarais et al.,
675 2015). Muropeptide labels: M = monomer, D = dimer, T = trimer, Q = tetramer; (3, 4, 5) indicate
676 the number of amino acid stem residues; modifications: G = glycine replacing L-alanine, LD =
677 3,3-diaminopimelic acid DAP-DAP cross-bridge, N = terminating anhydro-muropeptide, NN =
678 di-anhydro-muropeptides. Values represent the molar fraction of each muropeptide. The degree
679 of crosslinking was calculated as previously described (Glauner, 1988). Data are the means of
680 two biological replicates; standard deviations (s.d.) are in parentheses.

	Whole cell		Whole cell	
M3	0.50	(0.2)	1.53	(0.5)
M4	28.60	(2.2)	25.04	(5)
M5G	1.21	(1.5)	0.67	(0)
M5	24.59	(1.2)	17.94	(0.1)
D33LD	0.00	(0)	0.12	(0)
D43LD	0.03	(0)	1.89	(0.2)
D43	0.48	(0.1)	0.26	(0.1)
D44LD	0.11	(0)	0.29	(0.1)
D45G	0.17	(0)	0.28	(0.4)
D44	10.06	(1.4)	11.25	(2)
D45	9.95	(0.4)	11.82	(0.1)
T443LD	0.02	(0)	0.14	(0)
M4N	0.05	(0.1)	0.37	(0.1)
T444	1.74	(0.2)	2.25	(0.3)
T445G	1.57	(0)	2.19	(0.3)
M5N	0.93	(0.1)	1.78	(0.1)
D44N	0.34	(0)	0.70	(0)
D45GN	2.56	(0.2)	2.81	(0.3)
T443NLD	1.18	(0.4)	1.33	(0.3)
T444N	3.24	(0.2)	3.13	(0.2)
T445GN	2.87	(0.3)	2.49	(0.6)
Q4445N	4.48	(0)	6.43	(1.2)
T444NN	0.42	(0.1)	0.35	(0)
Q4445NN	2.92	(0)	2.64	(3.2)
D44NN	1.92	(0.3)	1.31	(1.6)

T445NN	0.05	(0)	1.00	(0.5)
Monomers (total)	55.88	(0.6)	47.34	(5.3)
Dimers (total)	25.62	(1)	30.72	(0.3)
Trimers (total)	11.09	(0.3)	12.87	(1.1)
Tetramers (total)	7.41	(0)	9.07	(4.4)
Tripeptides (total)	1.15	(0.3)	3.21	(0.2)
Tetrapeptides (total)	57.44	(2.5)	59.25	(0.7)
Pentapeptides (total)	41.37	(2.2)	37.49	(0.9)
LD-crosslinks	0.47	(0.2)	1.64	(0.3)
Degree of crosslinking	25.68	(0.3)	30.66	(3.9)

Table 2. Muropeptide analyses of *C. crescentus* stalks. Stalk and cell-body muropeptides were isolated by mechanical shearing from the indicated *C. crescentus* strains grown in 1 μM phosphate and analyzed by HPLC (Methods). Values represent the molar fraction of each muropeptide. The degree of crosslinking was calculated as previously described (Glauner, 1988). Data are the means of at least two biological replicates; s.d. are in parentheses.

	Wildtype Cell body		**Wildtype Stalk**		**Δ*ldtD* Stalk**		**Δ*ykuD* Stalk**		**Δ*ldtD* Δ*ykuD* Stalk**	
M3	1.40	(0.4)	4.61	(3)	0.37	(0)	1.88	(0)	0.69	(0.1)
M4	37.53	(7.2)	15.15	(0.1)	21.18	(2.3)	12.68	(0.7)	18.06	(1.1)
M5G	1.55	(1.1)	6.37	(5.5)	3.97	(0.3)	11.82	(0.6)	6.63	(0.5)
M5	15.22	(2.7)	13.31	(1.5)	14.61	(2.1)	12.66	(0.9)	14.91	(1.2)
D33LD	0.13	(0.1)	0.70	(0.2)	0.18	(0.1)	1.44	(0.1)	0.48	(0)
D43LD	1.49	(0.9)	4.13	(1.2)	0.00	(0)	5.41	(0.3)	0.00	(0)
D43	0.33	(0.2)	0.52	(0.3)	0.29	(0.3)	0.72	(0)	0.89	(0.1)
D44LD	0.24	(0.2)	0.57	(0.2)	0.00	(0)	0.21	(0)	0.10	(0)
D45G	0.39	(0.3)	0.13	(0.2)	0.47	(0.5)	0.59	(0)	0.11	(0)
D44	16.33	(3.8)	8.91	(0.5)	9.93	(0.3)	9.03	(0.5)	9.84	(0.6)
D45	9.47	(2)	9.14	(1)	9.87	(1.6)	9.30	(0.5)	11.10	(0.6)
T443LD	0.12	(0.1)	0.41	(0.2)	0.00	(0)	0.72	(0)	0.00	(0)
M4N	0.30	(0.1)	0.74	(0.3)	0.93	(0.7)	1.60	(0.3)	0.53	(0)
T444	2.74	(0.4)	3.36	(0.5)	3.08	(0.2)	3.45	(0.1)	3.92	(0.3)
T445G	1.38	(0.4)	2.59	(0.3)	3.23	(0.8)	2.90	(0.2)	3.08	(0.2)
M5N	1.12	(0.5)	4.04	(1.5)	2.87	(0.6)	4.42	(0.3)	4.43	(0.3)
D44N	0.57	(0.1)	2.12	(1.2)	2.08	(2.1)	2.02	(0.3)	1.81	(0.1)
D45GN	2.30	(0.5)	2.53	(1.1)	4.37	(1.1)	2.76	(0.1)	0.99	(0.1)
T443NLD	0.13	(0.1)	0.67	(0.3)	0.57	(0.6)	0.77	(0.1)	1.19	(0.1)
T444N	2.09	(0.8)	3.40	(0.2)	3.66	(0.3)	2.53	(0.1)	3.44	(0.2)
T445GN	1.06	(0.9)	3.36	(0.9)	4.16	(1.4)	2.21	(0.1)	2.83	(0.2)
Q4445N	2.18	(1.9)	5.70	(2.6)	8.04	(0.5)	6.66	(0.3)	8.34	(0.5)
T444NN	0.19	(0.2)	0.58	(0.3)	0.39	(0.3)	1.13	(1.4)	0.32	(0.1)
Q4445NN	1.02	(1.1)	5.09	(3.9)	2.69	(2.1)	2.46	(3.2)	5.67	(5.4)
D44NN	0.44	(0.4)	1.18	(0.8)	2.43	(0.3)	0.21	(0.2)	0.43	(0.3)
T445NN	0.28	(0.4)	0.71	(0.4)	0.62	(0.7)	0.40	(0.3)	0.20	(0.1)
Monomers (total)	57.11	(3.7)	44.22	(2.7)	43.93	(0.7)	45.06	(2.3)	45.25	(3.1)
Dimers (total)	31.70	(2.3)	29.93	(2.2)	29.63	(5)	31.70	(1.7)	25.75	(1.1)
Trimers (total)	7.99	(2.3)	15.07	(1.6)	15.71	(2.7)	14.12	(1)	14.99	(0.7)
Tetramers (total)	3.20	(3)	10.78	(6.5)	10.73	(1.6)	9.13	(2.9)	14.01	(4.9)
Tripeptides (total)	2.53	(0.8)	7.99	(2.6)	0.89	(0.1)	6.88	(0.4)	2.02	(0.1)
Tetrapeptides (total)	63.81	(4)	53.03	(1.8)	60.16	(2.1)	49.51	(1.9)	55.46	(1.5)
Pentapeptides (total)	33.64	(4.5)	38.93	(4.3)	38.89	(2.2)	43.56	(1.6)	42.47	(1.4)
LD-crosslinks	1.02	(0.6)	3.06	(0.7)	0.28	(0.2)	4.03	(0.3)	0.69	(0)
Degree of cross-linkage	23.52	(2.9)	33.00	(2.7)	33.23	(0.5)	32.01	(2)	33.28	(2.6)

687 **Figure Legends**

688

689 **Figure 1. *C. crescentus* stalks are resistant to enzymatic degradation.**

690 (A) *C. crescentus* cells were grown in HIGG + 30 µM phosphate, spheroplasted with 25 µg mL^{-1}
691 lysozyme for 15 min and imaged via negative staining transmission electron microscopy.
692 Lysozyme caused swelling of the cell body with no apparent effect on the stalk. Scale bar: 500
693 nm. (B) Strain EK182, which encodes xylose-inducible periplasmic tdimer2 fluorescent protein,
694 was grown overnight in HIGG + 1 µM phosphate with 0.3% xylose and 0.25 mM HADA.
695 Permeabilized cells were treated with 25 µg mL^{-1} lysozyme for 15 min. Lysozyme efficiently
696 digested the cell body as stalks remained intact. Scale bar: 5 µm. (C) NA1000 cells were grown
697 in HIGG + 1 µM phosphate with 0.25 mM HADA. Permeabilized cells were treated with 5 µM
698 Tae3 for 3 h. As with lysozyme, Tae3 did not degrade the stalk. (D) Permeabilized NA1000 cells
699 grown in HIGG + 1 µM phosphate were labeled with KZ144-YFP. KZ144-YFP labeling was
700 restricted to the cell body. Scale bar: 5 µm. (E) Muropeptides were purified from NA1000
701 grown in HIGG with 1 mM or 1 µM phosphate and analyzed via HPLC. The arrow indicates a
702 peak uniquely present in the 1 µM phosphate chromatogram. (F) DD-crosslinks, which are
703 targeted by Tae3, occur between *meso*-DAP and D-alanine residues of neighboring peptide
704 stems. LD-crosslinks, in contrast, are *meso*-DAP-*meso*-DAP linkages, which are not cut by Tae3.

705

706 **Figure 2. LD-transpeptidation is restricted to the stalk compartment.**

707 Isolation of purified stalks confirmed enrichment of LD-crosslinks in the stalk. Cells were grown
708 in HIGG + 1 µM phosphate and stalks were separated from cell bodies using two methods. Top:
709 YB2811 cells spontaneously shed their stalks into the medium. Bottom: NA1000 cells were

710 mechanically sheared in a blender to detach stalks. Muropeptides were purified from stalks and
711 cell bodies, and analyzed via HPLC. Isolated stalks were enriched for several LD-muropeptide
712 species as indicated.
713
714 **Figure 3. LdtD is responsible for LD-transpeptidation in the stalk.**
715 (A) Stalk muropeptides were analyzed by mechanically shearing stalks of wild-type and Δ*ldtD*
716 cells grown in HIGG + 1 μM phosphate. LD-crosslinked dimers are labeled. (B) Expression of
717 the LD-transpeptidase *ldtD* increased during phosphate starvation. *: $p<0.05$, one-tailed *t*-test,
718 error bars are standard error for three biological replicates. LdtD protein levels were quantified
719 by fluorescence microscopy. Cells with LdtD-mCherry expressed from the native promoter
720 (strain GS42) were imaged and the total fluorescence intensity of each cell was normalized to its
721 area. **: $p<0.001$, one-tailed *t*-test, error bars are standard error of the mean for $n>150$ cells. (C)
722 LdtD localization was determined to be approximately uniform using a C-terminal mCherry
723 fusion. *ldtD-mCherry* was integrated into the chromosome at the *xylX* locus for inducible
724 expression (top) or at the native locus for endogenous expression (bottom). Cells were grown in
725 HIGG + 1 μM phosphate with 0.3% xylose as indicated prior to fluorescence imaging. Scale bar:
726 5 μm. (D) Muropeptides were purified from wild-type and *ldtD*::*ldtD-mCherry* cells grown in
727 HIGG + 1 μM phosphate and analyzed via HPLC. The presence of LD-crosslinked dimers
728 (arrow) confirms that LdtD-mCherry is functional.
729
730 **Figure 4. LD-crosslinking mediates lysozyme sensitivity and KZ144-YFP binding.** (A)
731 NA1000 (wild-type) and Δ*ldtD* cells were grown in HIGG + 1 μM phosphate with 0.25 mM
732 HADA, permeabilized, and treated with 25 μg mL^{-1} lysozyme for 15 min. Wild-type stalks were

733 resistant to lysozyme digestion (arrowheads), while Δ*ldtD* stalks were fully degraded. Scale bar:
734 10 µm. (B) NA1000 wild-type and Δ*ldtD* cells were grown in HIGG + 1 µM phosphate and
735 labeled with KZ144-YFP. In contrast to wild-type cells, Δ*ldtD* stalks were labeled by KZ144-
736 YFP (arrowheads). Scale bar: 10 µm. (C-D) Permeabilized *A. tumefaciens* and *H. neptunium*
737 cells were labeled with KZ144-YFP. (C) The fluorescence intensity along the periphery of
738 elongating cells was normalized to the maximum fluorescence intensity. Elongating cells were
739 identified based on having unequal widths at the two poles. The narrower, growing pole
740 (asterisks) was identified via phase microscopy. Fluorescence intensity was highest at the
741 growing pole. Scale bar: 5 µm. (D) Unlike *C. crescentus*, the stalks of *H. neptunium* were labeled
742 by KZ144-YFP (arrowheads). Scale bar: 5 µm.
743
744 **Figure 5. LD-crosslinking correlates with resistance to lysozyme-mediated degradation.** (A)
745 Log-phase *E. coli*, stationary-phase *E. coli*, and log-phase *A. tumefaciens* cells were
746 permeabilized and digested with 1 µg mL^{-1} lysozyme at room temperature. The turbidity of the
747 treated samples was measured over time as the optical density at 600 nm. Control samples were
748 not treated with lysozyme, and each sample was normalized to its initial OD_{600}. Error bars are
749 standard error of a minimum of three biological replicates. (B) The initial velocities of lysozyme
750 activity were quantified by calculating the slopes of the curves in (A) during the interval from 0-
751 60 s. Error bars are standard error of a minimum of three biological replicates. Percentages of
752 LD-crosslinks were taken from published values (Brown et al., 2012, Pisabarro et al., 1985).
753 Comparing the rates of lysozyme-mediated degradation in these different species and growth
754 conditions demonstrated a correlation between a higher proportion of LD-crosslinks and
755 lysozyme resistance.

Figure 1

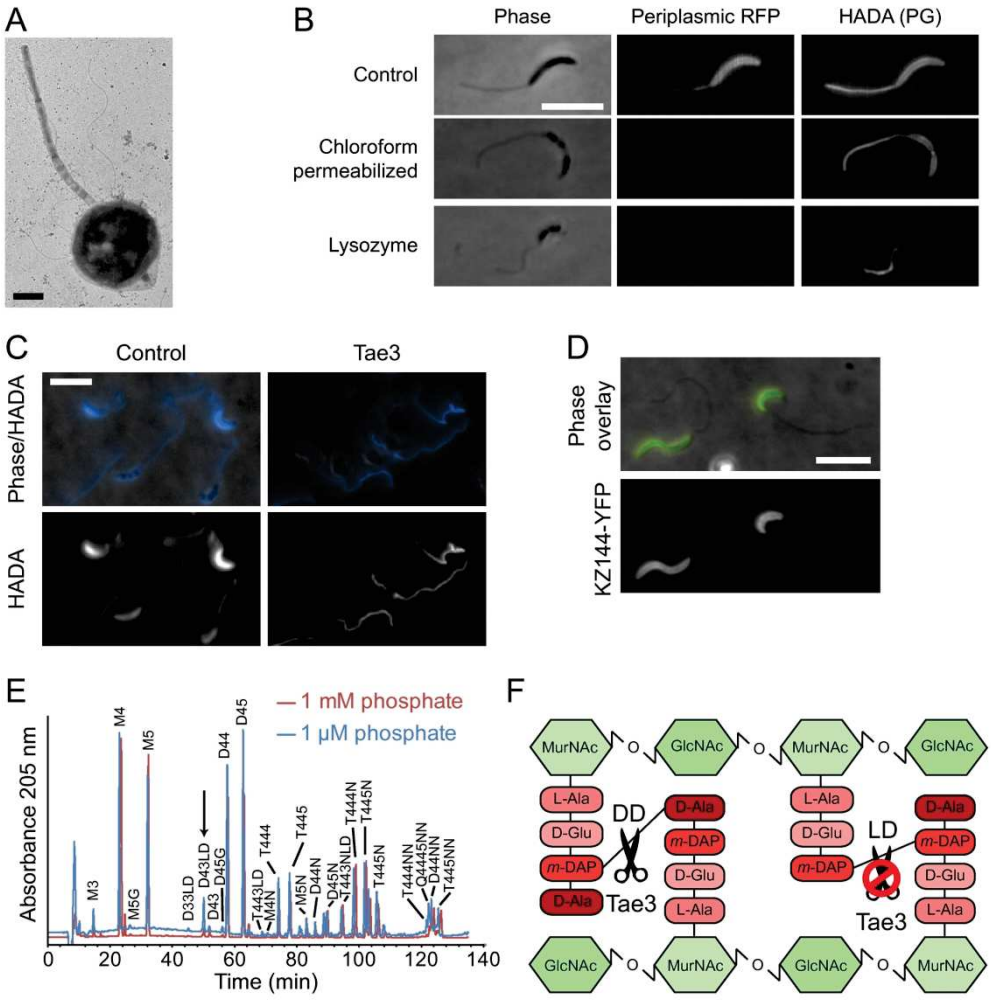

Figure 1. C. crescentus stalks are resistant to enzymatic degradation.
(A) C. crescentus cells were grown in HIGG + 30 μM phosphate, spheroplasted with 25 μg mL-1 lysozyme for 15 min and imaged via negative staining transmission electron microscopy. Lysozyme caused swelling of the cell body with no apparent effect on the stalk. Scale bar: 500 nm. (B) Strain EK182, which encodes xylose-inducible periplasmic tdimer2 fluorescent protein, was grown overnight in HIGG + 1 μM phosphate with 0.3% xylose and 0.25 mM HADA. Permeabilized cells were treated with 25 μg mL-1 lysozyme for 15 min. Lysozyme efficiently digested the cell body as stalks remained intact. Scale bar: 5 μm. (C) NA1000 cells were grown in HIGG + 1 μM phosphate with 0.25 mM HADA. Permeabilized cells were treated with 5 μM Tae3 for 3 h. As with lysozyme, Tae3 did not degrade the stalk. (D) Permeabilized NA1000 cells grown in HIGG + 1 μM phosphate were labeled with KZ144-YFP. KZ144-YFP labeling was restricted to the cell body. Scale bar: 5 μm. (E) Muropeptides were purified from NA1000 grown in HIGG with 1 mM or 1 μM phosphate and analyzed via HPLC. The arrow indicates a peak uniquely present in the 1 μM phosphate chromatogram. (F) DD-crosslinks, which are targeted by Tae3, occur between meso-DAP and D-alanine residues of neighboring peptide stems. LD-crosslinks, in contrast, are meso-DAP-meso-DAP linkages, which are not cut by Tae3.

168x189mm (300 x 300 DPI)

Figure 2

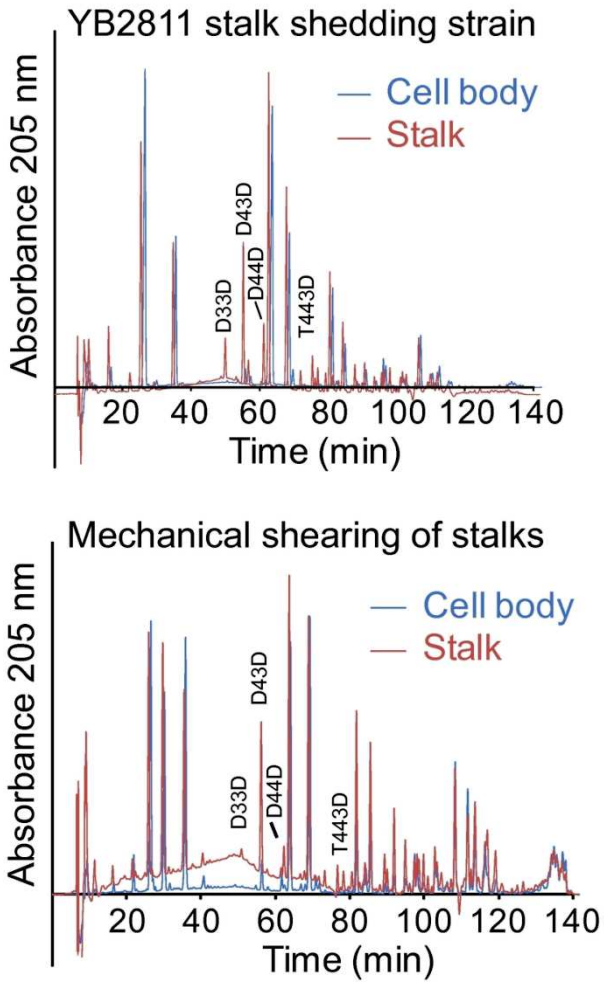

Figure 2. LD-transpeptidation is restricted to the stalk compartment.
Isolation of purified stalks confirmed enrichment of LD-crosslinks in the stalk. Cells were grown in HIGG + 1 μM phosphate and stalks were separated from cell bodies using two methods. Top: YB2811 cells spontaneously shed their stalks into the medium. Bottom: NA1000 cells were mechanically sheared in a blender to detach stalks. Muropeptides were purified from stalks and cell bodies, and analyzed via HPLC. Isolated stalks were enriched for several LD-muropeptide species as indicated.

80x139mm (300 x 300 DPI)

Figure 3

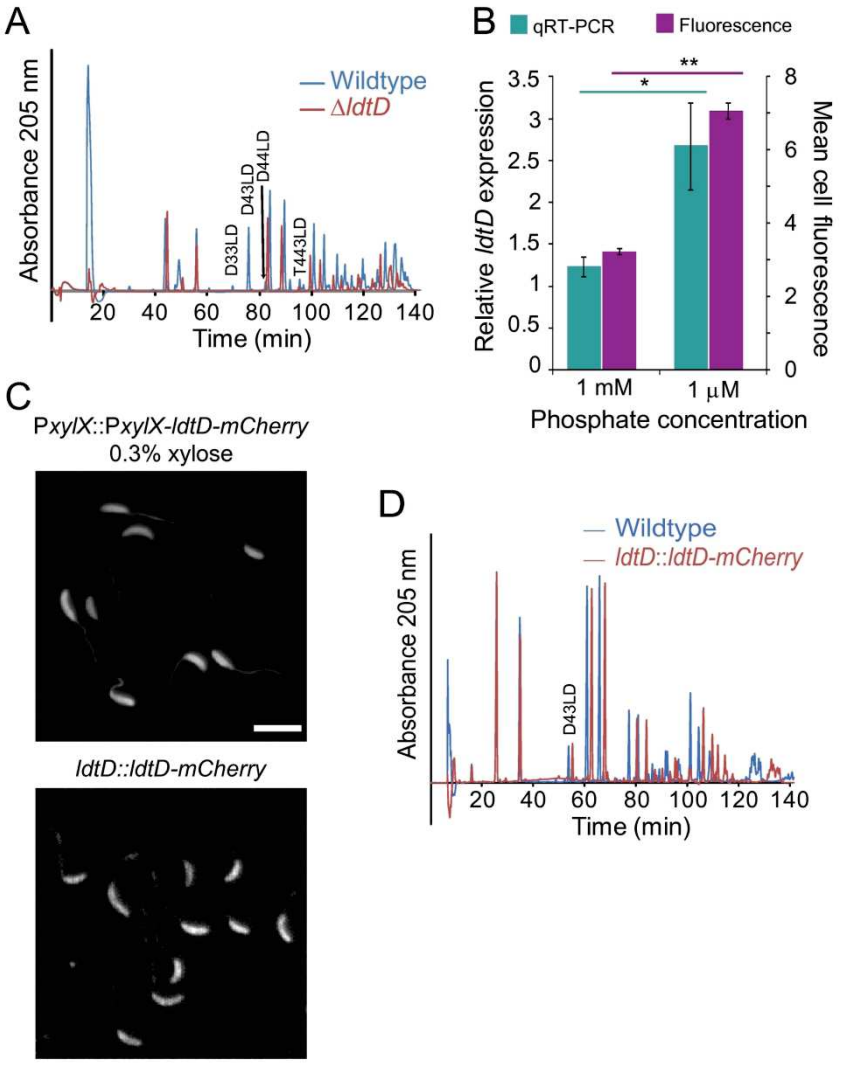

Figure 3. LdtD is responsible for LD-transpeptidation in the stalk.
(A) Stalk muropeptides were analyzed by mechanically shearing stalks of wild-type and ΔldtD cells grown in HIGG + 1 μM phosphate. LD-crosslinked dimers are labeled. (B) Expression of the LD-transpeptidase ldtD increased during phosphate starvation. *: $p<0.05$, one-tailed t-test, error bars are standard error for three biological replicates. LdtD protein levels were quantified by fluorescence microscopy. Cells with LdtD-mCherry expressed from the native promoter (strain GS42) were imaged and the total fluorescence intensity of each cell was normalized to its area. **: $p<0.001$, one-tailed t-test, error bars are standard error of the mean for $n>150$ cells. (C) LdtD localization was determined to be approximately uniform using a C-terminal mCherry fusion. ldtD-mCherry was integrated into the chromosome at the xylX locus for inducible expression (top) or at the native locus for endogenous expression (bottom). Cells were grown in HIGG + 1 μM phosphate with 0.3% xylose as indicated prior to fluorescence imaging. Scale bar: 5 μm. (D) Muropeptides were purified from wild-type and ldtD::ldtD-mCherry cells grown in HIGG + 1 μM phosphate and analyzed via HPLC. The presence of LD-crosslinked dimers (arrow) confirms that LdtD-mCherry is functional.

168x197mm (300 x 300 DPI)

Figure 4

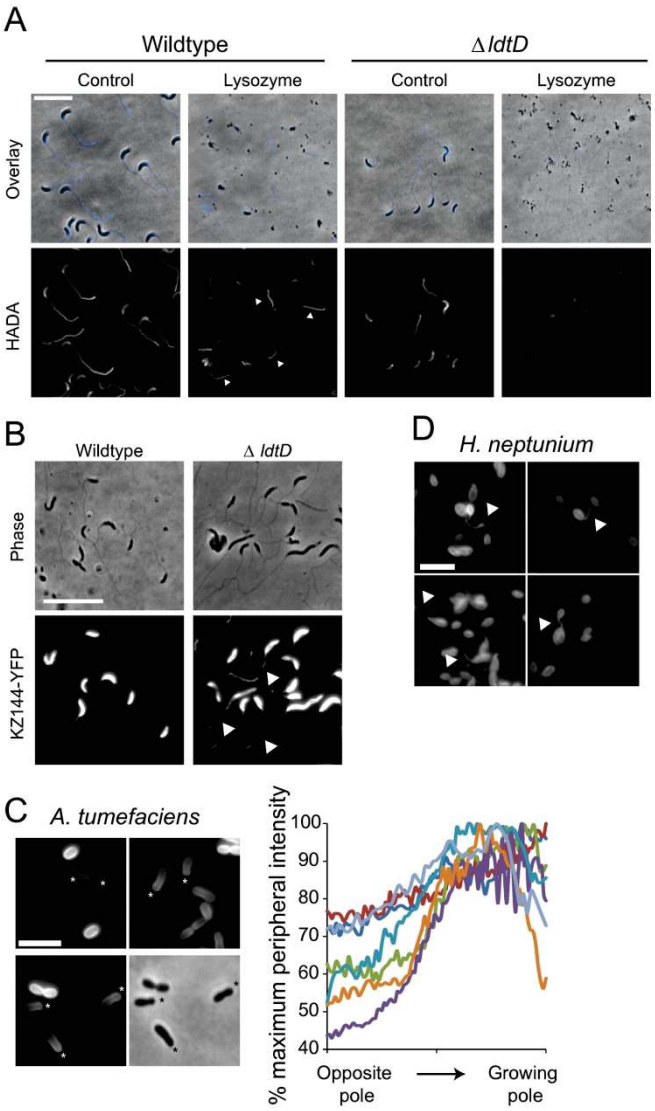

Figure 4. LD-crosslinking mediates lysozyme sensitivity and KZ144-YFP binding. (A) NA1000 (wild-type) and ☐ldtD cells were grown in HIGG + 1 μM phosphate with 0.25 mM HADA, permeabilized, and treated with 25 μg mL-1 lysozyme for 15 min. Wild-type stalks were resistant to lysozyme digestion (arrowheads), while ΔldtD stalks were fully degraded. Scale bar: 10 μm. (B) NA1000 wild-type and ΔldtD cells were grown in HIGG + 1 μM phosphate and labeled with KZ144-YFP. In contrast to wild-type cells, ΔldtD stalks were labeled by KZ144-YFP (arrowheads). Scale bar: 10 μm. (C-D) Permeabilized A. tumefaciens and H. neptunium cells were labeled with KZ144-YFP. (C) The fluorescence intensity along the periphery of elongating cells was normalized to the maximum fluorescence intensity. Elongating cells were identified based on having unequal widths at the two poles. The narrower, growing pole (asterisks) was identified via phase microscopy. Fluorescence intensity was highest at the growing pole. Scale bar: 5 μm. (D) Unlike C. crescentus, the stalks of H. neptunium were labeled by KZ144-YFP (arrowheads). Scale bar: 5 μm.

168x224mm (300 x 300 DPI)

Figure 5

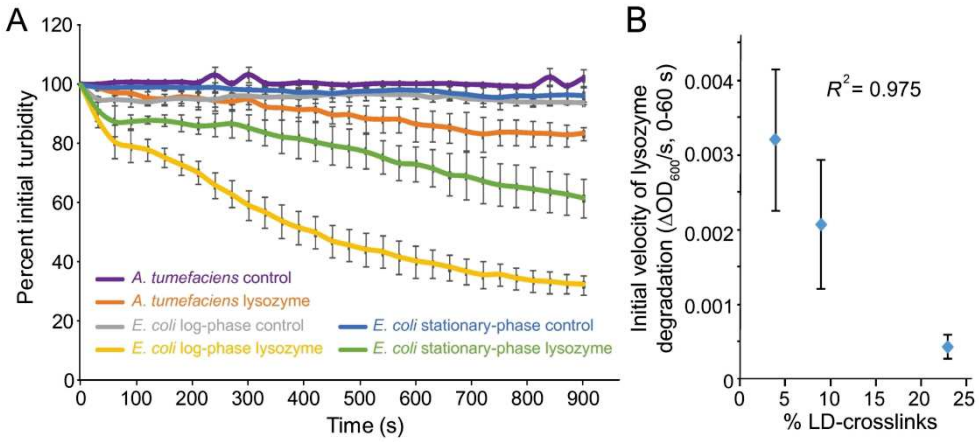

Figure 5. LD-crosslinking correlates with resistance to lysozyme-mediated degradation. (A) Log-phase E. coli, stationary-phase E. coli, and log-phase A. tumefaciens cells were permeabilized and digested with 1 µg mL-1 lysozyme at room temperature. The turbidity of the treated samples was measured over time as the optical density at 600 nm. Control samples were not treated with lysozyme, and each sample was normalized to its initial OD600. Error bars are standard error of a minimum of three biological replicates. (B) The initial velocities of lysozyme activity were quantified by calculating the slopes of the curves in (A) during the interval from 0-60 s. Error bars are standard error of a minimum of three biological replicates. Percentages of LD-crosslinks were taken from published values (Brown et al., 2012, Pisabarro et al., 1985). Comparing the rates of lysozyme-mediated degradation in these different species and growth conditions demonstrated a correlation between a higher proportion of LD-crosslinks and lysozyme resistance.

168x91mm (300 x 300 DPI)

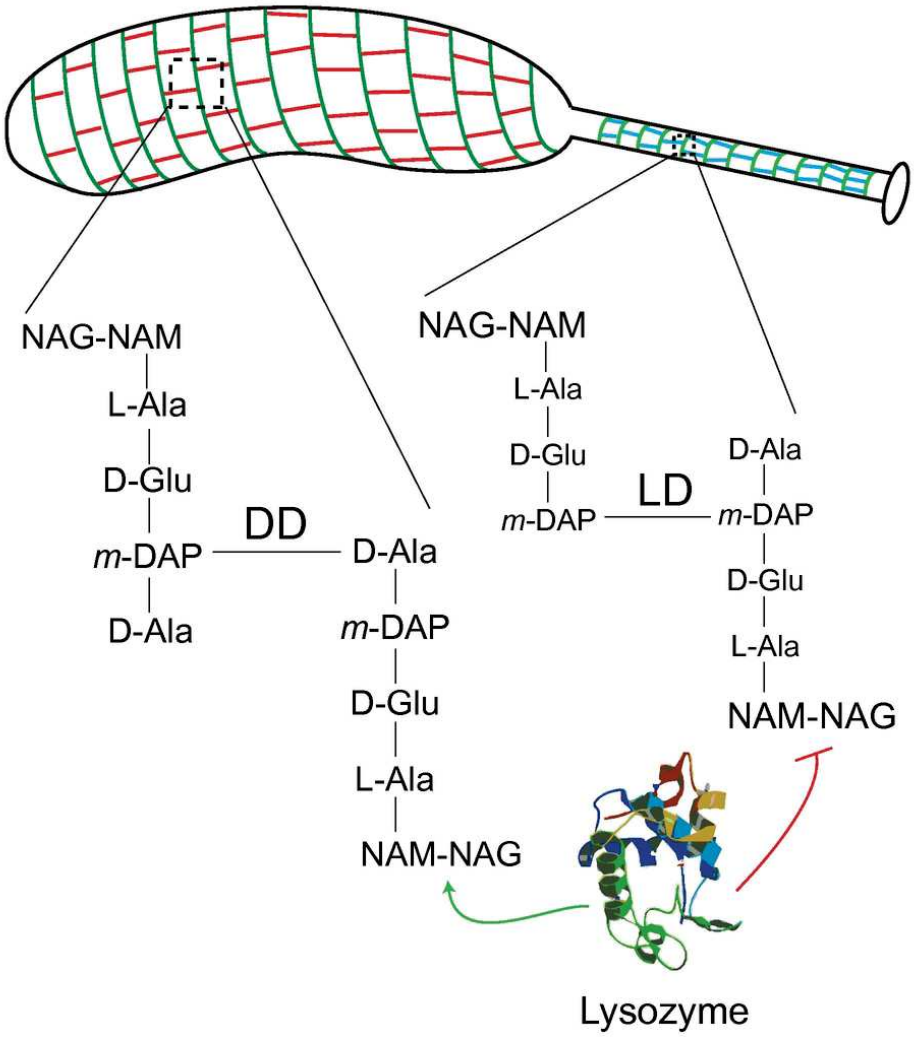

80x99mm (300 x 300 DPI)

Caulobacter crescentus forms a polar stalk with peptidoglycan composition distinct from that of the cell body. The stalk is enriched in DAP-DAP crosslinks mediated by the LD-transpeptidase LdtD. Elevated levels of LD-crosslinking provide resistance against lysozyme-mediated degradation in *C. crescentus* stalks, and this mechanism of lysozyme resistance may apply broadly to a variety of bacterial species.